RESEARCH ARTICLE • OPEN ACCESS

Mathematical Modeling of Cholera Transmission Capturing Vaccine Effect and Age Structure Using Homotopy Perturbation Method

Mutairu K. Kolawole and Segun R. Adebayo

Volume 13, Issue 2, pp. 157–168, Aug. 2025

Received 11 May 2025, Revised 4 June 2025, Accepted 5 June 2025, Published 1 July 2025

To Cite this Article : M. K. Kolawole and S. R. Adebayo,"Mathematical Modeling of Cholera Transmission Capturing Vaccine Effect and Age Structure Using Homotopy Perturbation Method", *Euler J. Ilm. Mat. Sains dan Teknol.*, vol. 13, no. 2, pp. 157–168, 2025, *https://doi.org/10.37905/euler.v13i2.31580*

JOURNAL INFO • EULER : JURNAL ILMIAH MATEMATIKA, SAINS DAN TEKNOLOGI

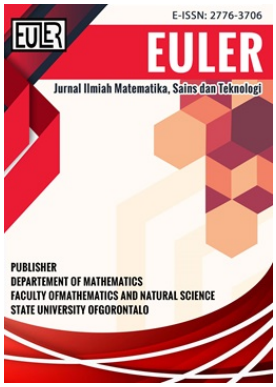

Homepage	:	http://ejurnal.ung.ac.id/index.php/euler/index
Journal Abbreviation	:	Euler J. Ilm. Mat. Sains dan Teknol.
Frequency	:	Three times a year
Publication Language	:	English (preferable), Indonesia
DOI	:	https://doi.org/10.37905/euler
Online ISSN	:	2776-3706
Publisher	:	Department of Mathematics, Universitas Negeri Gorontalo
Country	:	Indonesia
OAI Address	:	http://ejurnal.ung.ac.id/index.php/euler/oai
Google Scholar ID	:	QF_r-_gAAAAJ
Email	:	euler@ung.ac.id

JAMBURA JOURNAL • FIND OUR OTHER JOURNALS

Jambura Journal of Biomathematics

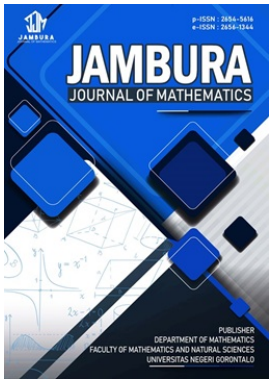

Jambura Journal of Mathematics

Jambura Journal of Mathematics Education

Jambura Journal of Probability and Statistics

Euler : Jurnal Ilmiah Matematika, Sains dan Teknologi, Volume 13, Issue 2, Pages 157–168, Aug. 2025 *https://doi.org/10.37905/euler.v13i2.31580*

Research Article

Mathematical Modeling of Cholera Transmission Capturing Vaccine Effect and Age Structure Using Homotopy Perturbation Method

Mutairu K. Kolawole[1], **Segun R. Adebayo** [1,*]

[1] *College of Science and Technology, Department of Mathematical Sciences, Osun State University, Osogbo, Nigeria*

ARTICLE HISTORY
Received 11 May 2025
Revised 4 June 2025
Accepted 5 June 2025
Published 1 July 2025

KEYWORDS
Cholera Disease
Vaccination
Basic Reproduction Number
Age Structure
Stability Analysis
Homotopy Perturbation Method

ABSTRACT. *This research presents a detailed mathematical model for cholera transmission, incorporating age structure and vaccine effects. The model is analysed using mathematical methods to examine the disease-free and endemic equilibria, positivity, existence, uniqueness, and well-posedness of the epidemic model. The basic reproduction number is calculated, helping to assess cholera's transmission potential and the effectiveness of interventions. Local stability analyses around the disease-free and endemic equilibria provide insights into the system's behavior under different conditions, while global stability analyses determine the long-term behavior of the epidemic. Sensitivity analysis, conducted using the homotopy perturbation method, evaluates how variations in model parameters affect disease dynamics. By integrating age structure and vaccination into the model, the study explores how demographic factors influence cholera control strategies. The model's uniqueness is mathematically proven, ensuring the reliability of the results. Overall, this research advances the understanding of cholera dynamics, offering insights for designing sustainable and effective public health interventions to control the disease by health practitioners.*

1. Introduction

Cholera is a severe infectious disease caused by the bacterium Vibrio cholerae. Its history is deeply intertwined with the development of human civilization, marked by catastrophic outbreaks and significant advancements in the understanding of its etiology and prevention strategies [1]. The disease is believed to have originated in the Ganges Delta in India, where it has been documented for centuries. However, it was not until the 19th century that cholera began to spread globally via trade and travel routes, eventually becoming one of the most lethal diseases of that period [2]. The first recorded cholera pandemic occurred in 1817, originating in India and spreading to Asia, Europe, and North America. This was followed by several other pandemics that caused widespread mortality and disrupted societies across continents.

Cholera is primarily transmitted through the ingestion of contaminated water and food sources [3]. Poor sanitation infrastructure and limited access to clean water are the leading contributors to the continued transmission of the disease, especially in vulnerable communities [4]. The bacterium produces an enterotoxin that induces profuse watery diarrhea and severe dehydration, which, if not promptly treated, can result in rapid fluid loss and death [5, 6]. Additional symptoms often include vomiting, an accelerated heart rate, and hypotension [7]. Without immediate and adequate rehydration therapy, cholera can become fatal within a matter of hours. Human practices such as improper waste disposal and the discharge of untreated sewage into water bodies further exacerbate water contamination and maintain the cycle of transmission [8].

Furthermore, environmental changes linked to climate change may intensify cholera outbreaks by altering key ecological conditions. Rising temperatures and shifting rainfall patterns influence water quality and create favorable conditions for bacterial proliferation [9]. Although cholera can affect individuals of all ages, children are particularly susceptible due to their weaker immune systems and smaller body size, which make them more vulnerable to severe dehydration and its complications [10, 11]. Children also tend to be disproportionately impacted by poor sanitation and limited access to healthcare services in low-resource settings where cholera outbreaks are common [12].

Today, cholera remains a significant global health concern, especially in regions struggling with inadequate sanitation and unsafe drinking water [13]. In this context, mathematical modeling has become an indispensable tool for analyzing the transmission dynamics of cholera and assessing the potential impact of various intervention strategies, such as vaccination programs [14–17]. Models that incorporate age structure and vaccine effects are crucial for accurately evaluating the effectiveness of such interventions. The use of human population movement models provides a powerful analytical framework for understanding how demographic variables like age distribution and mobility patterns influence the spread of cholera [18].

By integrating vaccine efficacy into these models, researchers can simulate the outcomes of targeted vaccination campaigns and their potential to reduce disease incidence and prevalence across different age cohorts and geographical areas [19, 20]. This comprehensive modeling approach allows for

* Corresponding Author.

Email : *adebayosegunraphael@gmail.com* (S. R. Adebayo)
Homepage : http://ejurnal.ung.ac.id/index.php/euler/index / E-ISSN : 2776-3706

the examination of age-specific vaccination strategies and their role in curbing cholera transmission. Furthermore, mathematical models utilizing the homotopy perturbation method can capture the intricate interplay among age structure, population movement, and vaccine efficacy. Such models offer valuable insights that support the development and implementation of effective, targeted public health interventions to combat cholera on a global scale [21–23].

2. Model

The total population $N(t)$ is distinctly divided into seven sub-compartments with the following population sizes: susceptible children (S_c), susceptible adults (S_a), vaccinated individuals (V), infected individuals (I), quarantined individuals (Q), recovered individuals (R), and the bacterial population in the environment (B).

The recruitment (inflow) of children and adults into the population is denoted by Λ_c and Λ_a, respectively. Cholera transmission occurs at a rate α, as individuals become exposed through contact with contaminated water. The implementation of hygiene practices reduces the effective contact rate and the risk of disease transmission. The hygiene rate among individuals and the maturation rate at which children transition into the adult class are governed by parameters ρ_1 and ρ_2, respectively. Public health awareness efforts follow a logistic function that targets the infected population, with vaccination rates denoted by φ_1 and φ_2 for children and adults, respectively. Infected individuals are treated at a rate τ, with a recovery rate from cholera denoted by ε. Hospitalized individuals receive treatment under quarantine at a rate η.

More than 75% of *Vibrio cholerae* transmission risk is attributed to environmental contamination, which significantly contributes to the spread of the disease. Vaccination of susceptible individuals depends on both the vaccine efficacy and the bacterial shedding rate of the infected human population. Additionally, natural mortality rates for both humans and *V. cholerae* are represented by the parameter μ.

These dynamics are captured through a schematic flow diagram and a system of nonlinear differential equations, as presented in eq. (1) below. By incorporating age structure and vaccination strategies through Λ_c and Λ_a, we model the recruitment of individuals into the susceptible children and adult compartments, respectively.

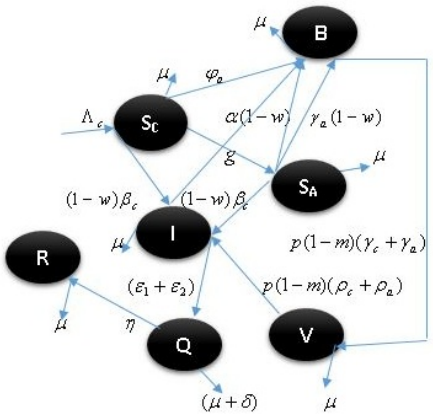

Figure 1. The schematic flow of the model formulation

Table 1. Variables of the model and description

Variable	Definition
S_c	Susceptible children population
S_a	Susceptible adult population
V	Vaccinated population
I	Infected population
Q	Quarantine population
R	Recovered population
B	Bacteria compartment

$$
\begin{aligned}
\frac{dS_c}{dt} &= \Lambda_c - (1-w)[\gamma_c B + \beta_c I]S_c - (\mu + \varphi - c)S_c - gS_c \\
\frac{dS_a}{dt} &= \Lambda_a - (1-w)[\gamma_a B + \beta_a I]S_a - (\mu + \varphi - a)S_a - gS_a \\
\frac{dV}{dt} &= \varphi_c S_c + \varphi_a S_a - p(1-m)[(\gamma_c + \gamma_a)B + (\beta_c + \beta_a I]V \\
&\quad - \mu V \\
\frac{dI}{dt} &= (1-w)[\gamma_c B + \beta_c I]S_c + (1-w)[\gamma_a B + \beta_a I]S_a \\
&\quad + \rho(1-m)[(\gamma_a + \gamma_c)B + (\beta_a + \beta_c)I] - AI \\
\frac{dQ}{dt} &= (\varepsilon_1 + \varepsilon_2)I - (\mu + \eta + \delta) \\
\frac{dR}{dt} &= \eta Q - \mu R \\
\frac{dB}{dt} &= \alpha(1-w)I - B\sigma
\end{aligned}
\tag{1}
$$

where $A = (\mu + \varepsilon_1 + \varepsilon_2 + \delta)$ subjected to the initial conditions $S(0)_c = s_o, S(0)_a = s_o, V(0) = v_o, I(0) = i_o, Q(0) = q_o, R(0) = r_o, B(0) = b_o$.

3. Results and Discussion

3.1. Existence and Uniqueness of the Model

Examining the population-related segment of the system of equations, we have

$$N(t) = S_c(t) + S_a(t) + V(t) + I(t) + Q(t) + R(t) + B(t).$$

The derivatives obtained as

$$\frac{dN(t)}{dt} = \frac{dS_c}{dt} + \frac{dS_a}{dt} + \frac{dV}{dt} + \frac{dI}{dt} + \frac{dQ}{dt} + \frac{dR}{dt} + \frac{dB}{dt}.$$

The total population $N(t)$ satisfies the differential inequality

$$\frac{dN(t)}{dt} \leq \Lambda_c + \Lambda_a - \mu N(t) - \delta I(t),$$

where Λ_c and Λ_a represent the recruitment rates of children and adults, respectively, and μ is the natural mortality rate. In the absence of a cholera outbreak, i.e., when $\delta = 0$, the inequality reduces to

$$\frac{dN(t)}{dt} + \mu N(t) \leq \Lambda,$$

where $\Lambda = \Lambda_c + \Lambda_a$. Multiplying both sides by the integrating factor $e^{\mu t}$, we obtain

$$\frac{d}{dt}\left[N(t)e^{\mu t}\right] \leq \Lambda e^{\mu t}.$$

Table 2. Parameters of the model and description

Parameters	Definition
Λ_c	recruitment rate into children susceptible population
Λ_a	recruitment rate into adult susceptible population
θ	vaccination rate
m	immunity level
φ_c, φ_a	vaccination rate of children and adult
α	contribution rate of infected to vibro amount in the population
δ	disease induced death
w	hygiene rate
σ	decay rate of vibro-cholera by adult
g	progression rate of children to adult
η	treatment rate of quarantine individual
γ_a, γ_c	ingestion rate of vibro-cholerae by children and adult population
μ	natural death
p	cholera modification parameter
$\varepsilon_1, \varepsilon_1$	quarantine rate of patients
ρ_1, ρ_2	waning rate of immunity

Integrating both sides with respect to t gives

$$N(t)e^{\mu t} \leq \frac{\Lambda e^{\mu t}}{\mu} + C,$$

where C is the constant of integration. Solving for $N(t)$, we have

$$N(t) \leq \frac{\Lambda}{\mu} + Ce^{-\mu t}.$$

By applying the initial condition at $t = 0$, the constant C is given by

$$C = N(0) - \frac{\Lambda}{\mu}.$$

Thus, as time progresses, the population $N(t)$ satisfies

$$\begin{aligned}\lim_{t\to\infty} N(t) &\leq \lim_{t\to\infty} \left[\frac{\Lambda}{\mu} + \left(N(0) - \frac{\Lambda}{\mu}\right) e^{-\mu t}\right] \\ &= \frac{\Lambda}{\mu}.\end{aligned}$$

Therefore, if $N(0) \leq \frac{\Lambda}{\mu}$, then $N(t) \leq \frac{\Lambda}{\mu}$ for all $t \geq 0$. This implies that the region $\mathbb{R}^7_+$ is positively invariant under the flow of the system, meaning no solution trajectory leaves the boundary of $\mathbb{R}^7_+$. Consequently, it is sufficient to consider the dynamics of the model within the domain $\mathbb{R}^7_+$.

In this region, the model is mathematically and epidemiologically well-posed, representing a physically meaningful problem. This result shows that the total population $N(t)$, composed of the sub-populations $S_c(t), S_a(t), V(t), I(t), Q(t), R(t)$, and $B(t)$, remains bounded and that the solution is unique.

3.2. *Positivity and Boundedness of the Model Solution*

From eq. (1), we derive the following conditions to verify the positivity of the model variables.

For the susceptible children compartment $S_c(t)$, we have:

$$\begin{aligned}\frac{dS_c}{dt} &= \Lambda_c - (1-w)[\gamma_c B + \beta_c I]S_c - (\mu + \varphi_c)S_c - gS_c, \\ \frac{dS_c}{dt} &\geq -\left[(1-w)(\gamma_c B + \beta_c I) + \mu + \varphi_c + g\right] S_c, \\ \frac{1}{S_c}\frac{dS_c}{dt} &\geq -\left[(1-w)(\gamma_c B + \beta_c I) + \mu + \varphi_c + g\right], \\ \int \frac{1}{S_c}\, dS_c &\geq -\int \left[(1-w)(\gamma_c B + \beta_c I) + \mu + \varphi_c + g\right] dt, \\ \ln S_c(t) &\geq -\left[(1-w)(\gamma_c B + \beta_c I) + \mu + \varphi_c + g\right] t + C_1, \\ S_c(t) &\geq e^{C_1} e^{-[(1-w)(\gamma_c B + \beta_c I) + \mu + \varphi_c + g]t} > 0.\end{aligned}$$

Hence, $S_c(t) > 0$ for all $t \geq 0$.

Similarly, for the susceptible adult compartment $S_a(t)$, we obtain:

$$\begin{aligned}\frac{dS_a}{dt} &= \Lambda_a - (1-w)[\gamma_a B + \beta_a I]S_a - (\mu + \varphi_a + g)S_a, \\ \frac{dS_a}{dt} &\geq -\left[(1-w)(\gamma_a B + \beta_a I) + \mu + \varphi_a + g\right] S_a, \\ \frac{1}{S_a}\frac{dS_a}{dt} &\geq -\left[(1-w)(\gamma_a B + \beta_a I) + \mu + \varphi_a + g\right], \\ \int \frac{1}{S_a}\, dS_a &\geq -\int \left[(1-w)(\gamma_a B + \beta_a I) + \mu + \varphi_a + g\right] dt, \\ \ln S_a(t) &\geq -\left[(1-w)(\gamma_a B + \beta_a I) + \mu + \varphi_a + g\right] t + C_2, \\ S_a(t) &\geq e^{C_2} e^{-[(1-w)(\gamma_a B + \beta_a I) + \mu + \varphi_a + g]t} > 0.\end{aligned}$$

Thus, $S_a(t) > 0$ for all $t \geq 0$.

For the vaccinated population $V(t)$, the positivity condition follows as:

$$\begin{aligned}\frac{dV}{dt} &= \Lambda_v - p(1-m)\left[(\gamma_c + \gamma_a)B + (\beta_c + \beta_a)I\right] V - \mu V, \\ \frac{dV}{dt} &\geq -\left[p(1-m)\left((\gamma_c + \gamma_a)B + (\beta_c + \beta_a)I\right) + \mu\right] V, \\ \frac{1}{V}\frac{dV}{dt} &\geq -\left[p(1-m)\left((\gamma_c + \gamma_a)B + (\beta_c + \beta_a)I\right) + \mu\right], \\ \int \frac{1}{V}\, dV &\geq -\int \left[p(1-m)\left((\gamma_c + \gamma_a)B + (\beta_c + \beta_a)I\right) + \mu\right] dt, \\ \ln V(t) &\geq -\left[p(1-m)\left((\gamma_c + \gamma_a)B + (\beta_c + \beta_a)I\right) + \mu\right] t + C_3, \\ V(t) &\geq e^{C_3} e^{-p(1-m)((\gamma_c+\gamma_a)B + (\beta_c+\beta_a)I)t} > 0.\end{aligned}$$

Therefore, $V(t) > 0$ for all $t \geq 0$.

By applying similar arguments, we conclude that the remaining state variables $I(t), Q(t), R(t), B(t)$ also remain positive for all $t \geq 0$. Hence, all solutions remain in the positive orthant $\mathbb{R}^7_+$. This confirms that the model is mathematically and epidemiologically well-posed and that the region $\mathbb{R}^7_+$ is positively invariant under the model dynamics.

3.3. Disease-Free Equilibrium

From the system of equations presented above, the disease-free equilibrium (DFE) corresponds to the state in which there is no cholera infection in the population, i.e., when $I(t) = 0$. At equilibrium, all derivatives with respect to time vanish, so we have:

$$\frac{dS_c}{dt} = \frac{dS_a}{dt} = \frac{dV}{dt} = \frac{dI}{dt} = \frac{dQ}{dt} = \frac{dR}{dt} = \frac{dB}{dt} = 0.$$

The resulting system of algebraic equations becomes:

$$\begin{aligned}
0 &= \Lambda_c - (1-w)(\gamma_c B + \beta_c I)S_c - (\mu + \varphi_c)S_c - gS_c,\\
0 &= \Lambda_a - (1-w)(\gamma_a B + \beta_a I)S_a - (\mu + \varphi_a)S_a - gS_a,\\
0 &= \varphi_c S_c + \varphi_a S_a - p(1-m)[(\gamma_c + \gamma_a)B + (\beta_c + \beta_a)I]V - \mu V,\\
0 &= (1-w)(\gamma_c B + \beta_c I)S_c + (1-w)(\gamma_a B + \beta_a I)S_a\\
&\quad + \rho(1-m)[(\gamma_c + \gamma_a)B + (\beta_c + \beta_a)I] - (\mu + \varepsilon_1 + \varepsilon_2 + \delta)I,\\
0 &= (\varepsilon_1 + \varepsilon_2)I - (\mu + \eta + \delta)Q,\\
0 &= \eta Q - \mu R,\\
0 &= \alpha(1-w)I - \sigma B.
\end{aligned}$$

At the disease-free equilibrium, we substitute $I = 0$, $Q = 0$, $R = 0$, and $B = 0$ into the system. Solving for the remaining variables, we obtain:

$$\begin{aligned}
S_c^0 &= \frac{\Lambda_c}{\mu + \varphi_c + g},\\
S_a^0 &= \frac{\Lambda_a(\mu + \varphi_c + g) - g\Lambda_c}{(\mu + \varphi_a + g)(\mu + \varphi_c)},\\
V^0 &= \frac{\varphi_c\Lambda_c(\mu + \varphi_a) - \varphi_a\Lambda_a(\mu + \varphi_c + g) - g\Lambda_c\varphi_c}{\mu(\mu + \varphi_c + g)(\mu + \varphi_a)},\\
I^0 &= Q^0 = R^0 = B^0 = 0.
\end{aligned}$$

Therefore, the disease-free equilibrium is given by the vector:

$$DFE = \left(S_c^0, S_a^0, V^0, 0, 0, 0, 0\right) \tag{2}$$

which represents the steady-state solution in the absence of cholera infection, indicating that the system is stable under no disease transmission.

3.4. Endemic Equilibrium Point

Let $E_e = (S_c^*, S_a^*, V^*, I^*, Q^*, R^*, B^*)$ denote the endemic equilibrium point of the model, where $I^* \neq 0$. At this equilibrium, the system reaches a steady state in the presence of the disease. The values of the state variables at the endemic equilibrium are given as follows:

$$S_c^* = \frac{\Lambda_c}{\Psi_c + \mu + g}, \tag{3}$$

$$S_a^* = \frac{\Lambda_a(\mu + \Psi_c + g) - g\Lambda_c}{(\mu + \Psi_c + g)(\mu + \Psi_a)}, \tag{4}$$

$$V^* = \frac{\Lambda_c\Psi_c(\mu + \Psi_c) - \Psi_a\Lambda_a(\mu + \Psi_c + g) - g\Lambda_c}{\mu\Psi_c(\mu + \Psi_c + g)(\mu + \Psi_a)}, \tag{5}$$

$$I^* = \frac{\Lambda_c\Psi_c(\mu + \Psi_c) - \Psi_a\Lambda_a(\mu + \Psi_c + g) + g\Lambda_c}{\mu\Psi_a(\mu + \Psi_a + g)(\mu + \Psi_a)}, \tag{6}$$

$$Q^* = \frac{(\mu + \Psi_a)\Lambda_c - g\Lambda_c(\Psi_c + g)}{\mu(\mu + \Psi_c + g)}, \tag{7}$$

$$R^* = \frac{\eta\left[(\mu + \Psi_a)\Lambda_c - g\Lambda_c(\Psi_c + g)\right]}{\mu(\mu + \Psi_c + g)}, \tag{8}$$

$$B^* = \frac{(\mu + \Psi_a + g) - (\Psi_a\Lambda_a + \Lambda_c)}{(\mu + \Psi_c + g)\Psi_a(\mu + \Psi_a)}. \tag{9}$$

These expressions define the endemic equilibrium in terms of the system parameters. The existence of a positive endemic equilibrium point implies the persistence of the disease within the population under certain conditions.

3.5. Basic Reproduction Number R_0

The basic reproduction number, denoted as R_0, quantifies the expected number of secondary infections produced by a single infectious individual in a completely susceptible population. To compute R_0, we apply the *next-generation matrix method* by considering the infected compartments of the system, namely: the exposed individuals (if included), the infected individuals (I), and the bacterial concentration in the environment (B).

This method involves constructing two matrices: **F**, which represents the rate of new infections, and **V**, which represents the transfer of individuals into and out of infected classes. These are derived from the system of equations at equilibrium (System (1)).

$$F_i = \left(\frac{\partial f_i(x)}{\partial x_j}\right), \qquad V_i = \left(\frac{\partial \nu_i(x)}{\partial x_j}\right),$$

where $i, j = 1, 2, \ldots, 7$, and f_i and ν_i represent the new infection terms and transition terms, respectively.

Assuming the model is reduced to two primary infectious components (I and B), the Jacobian matrices evaluated at the disease-free equilibrium are:

$$\begin{aligned}
\mathbf{F} &= \begin{pmatrix} 0 & \dfrac{\eta(\mu + \Psi_a)\Lambda_c}{\Lambda_c - g\Lambda_c(\Psi_c + g)} \\ 0 & 0 \end{pmatrix},\\
\mathbf{V} &= \begin{pmatrix} (1-w)(\beta_a + \beta_c) + \mu + \eta & 0 \\ -\kappa & \alpha + \mu + \gamma + \delta \end{pmatrix}.
\end{aligned}$$

Then, the next-generation matrix is given by:

$$\mathbf{FV}^{-1} = \frac{1}{[(\kappa + \mu)(\alpha + \gamma + \mu + \Psi_a)]} \begin{pmatrix} 0 & \dfrac{\eta(\mu + \Psi_a)\Lambda_c}{\Lambda_c - g\Lambda_c(\Psi_c + g)} \\ 0 & 0 \end{pmatrix} \begin{pmatrix} (1-w)(\beta_a + \beta_c) + \mu + \eta & 0 \\ -\kappa & \alpha + \mu + \gamma + \delta \end{pmatrix}.$$

The spectral radius (dominant eigenvalue) of the matrix $\mathbf{FV}^{-1}$ yields the basic reproduction number R_0, which is given by:

$$R_0 = \frac{(1-w)\left[\gamma_c\beta_c + \beta_a\Psi_a + \gamma_a\beta_a + \beta_c\Psi_c\right]}{(\mu+\varepsilon_1+\varepsilon_2+\delta)(\beta_a+\beta_c)}. \tag{10}$$

This expression reflects the contribution of both direct human-to-human transmission and indirect environment-mediated transmission to the overall reproduction number. The value of R_0 determines whether an outbreak will occur: if $R_0 > 1$, the disease can invade and persist in the population; if $R_0 < 1$, the disease will eventually die out.

3.6. Local Stability of Disease Free Equilibrium

Theorem 1. *The disease-free equilibrium (DFE) of the proposed cholera transmission model is locally asymptotically stable if $R_0 < 1$, and unstable if $R_0 > 1$.*

Proof. To determine the local stability of the DFE, we linearize the system around the disease-free equilibrium point E_0. The Jacobian matrix of the system defined in eq. (1), evaluated at the DFE, yields a characteristic equation of the form:

$$|J_{E_0} - \lambda I| = 0, \quad \lambda \in \mathbb{C}, \quad \text{with } \lambda_1, \lambda_2, \ldots, \lambda_7 \in \mathbb{R}.$$

Let us denote the Jacobian matrix evaluated at the DFE as:

$$J_{E_0} = \begin{bmatrix} A & 0 & 0 & a_{14} & 0 & 0 & a_{17} \\ g & B & 0 & a_{24} & 0 & 0 & a_{27} \\ \Psi_c & \Psi_a & C & a_{34} & 0 & 0 & 0 \\ a_{41} & a_{42} & 0 & D & 0 & 0 & 0 \\ 0 & 0 & 0 & \eta & -\mu & E & 0 \\ 0 & 0 & 0 & 0 & 0 & 0 & -\mu \end{bmatrix}$$

with:

$$\begin{aligned} a_{14} &= -\beta_c,\ a_{17} = \frac{\alpha}{\kappa},\ a_{24} = \beta S_a,\ a_{27} = \frac{\alpha}{\kappa}, \\ a_{34} &= \beta_c + \beta_a, \\ a_{41} &= \frac{(1-w)\beta_a\alpha\beta_c}{\kappa + B}, \\ a_{42} &= \frac{(1-w)\beta_a\alpha B + \beta_c}{\kappa + B}, \end{aligned}$$

Substituting $J_{E_0} - \lambda I$ and solving for the eigenvalues, we obtain:

$$\begin{aligned} \lambda_1 &= -\frac{(1-w)\alpha_c B + \beta_c + \mu + \Psi_c + g}{\kappa + B}, \\ \lambda_2 &= -\frac{B\alpha + \beta_a + \mu + \Psi_a}{\kappa + B}, \\ \lambda_3 &= -\frac{\rho(1-m)(\alpha_c + \alpha_a)B + (\beta_a + \beta_c)}{\kappa + B}, \\ \lambda_4 &= -(\beta_a + \beta_c + \mu + \varepsilon_1 + \varepsilon_2 + \delta), \\ \lambda_5 &= -\eta, \\ \lambda_6 &= -\mu, \\ \lambda_7 &= -\mu. \end{aligned}$$

Since all eigenvalues $\lambda_i < 0$ for $i = 1, \ldots, 7$ when $R_0 < 1$, this implies that the Jacobian matrix has all negative real parts, indicating that the DFE is locally asymptotically stable.

Biologically, this means that the infection will die out over time if appropriate control measures (such as vaccination, improved hygiene, and treatment) are implemented effectively. Mathematically, the region $\mathbb{R}^7_+$ is positively invariant under the flow of the system, and the stability condition holds provided that:

$$\forall \lambda_i < 0, \quad i = 1, \ldots, 7.$$

Hence, the disease-free equilibrium is locally asymptotically stable if $R_0 < 1$. □

3.7. Local Stability of the Endemic Equilibrium

Theorem 2. *The endemic equilibrium of the proposed cholera transmission model is locally asymptotically stable if $R_0 < 1$, and unstable otherwise.*

Proof. Let the perturbations around the endemic equilibrium be defined as:

$$\begin{aligned} S_c &= x + S_c^*, \quad S_a = y + S_a^*, \quad V = z + V^*, \\ I &= p + I^*, \quad Q = r + Q^*, \quad R = c + R^*, \\ B &= d + B^*. \end{aligned}$$

By linearizing the model equations around the endemic equilibrium, we obtain the following system of differential equations:

$$\begin{aligned} \frac{dS_c}{dt} &= -(1-w)(\gamma_c d + \beta_c p) - (\mu + \varphi_c)(x + S_c^*) - g(x + S_c^*), \\ \frac{dS_a}{dt} &= -(1-w)(\gamma_a d + \beta_a p)(y + S_a^*) - (\mu + \varphi_a)(y + S_a^*) \\ &\quad - g(y + S_a^*), \\ \frac{dV}{dt} &= \varphi_c(x + S_c^*) + \varphi_a(y + S_a^*) - p(1-m)\left[(\gamma_c + \gamma_a)d\right. \\ &\quad \left. + (\beta_c + \beta_a)p\right](z + V^*) - \mu(z + V^*), \\ \frac{dI}{dt} &= (1-w)(\gamma_c B + \beta_c I)(x + S_c^*) + (1-w)(\gamma_a B + \beta_a I) \\ &\quad (y + S_a^*) + \rho(1-m)[(\gamma_c + \gamma_a)B + (\beta_c + \beta_a)(p + I^*)] \\ &\quad + A, \\ \frac{dQ}{dt} &= (\varepsilon_1 + \varepsilon_2)(p + I^*) - (\mu + \eta + \delta)(r + Q^*), \\ \frac{dR}{dt} &= \eta(r + Q^*) - \mu(c + R^*), \\ \frac{dB}{dt} &= \alpha(1-w)(p + I^*) - \sigma(d + B^*), \end{aligned}$$

where the term $A = -(\mu + \varepsilon_1 + \varepsilon_2 + \delta)(p + I^*)$ accounts for the net loss from the infected class.

The Jacobian matrix of the system evaluated at the endemic equilibrium point E_e is given by:

$$J_{E_e} = \begin{bmatrix} A & 0 & 0 & -\beta_c & 0 & 0 & \frac{\alpha}{\kappa} \\ g & B & 0 & \beta S_a & 0 & 0 & \frac{\alpha}{\kappa} \\ \Psi_c & \Psi_a & C & \beta_c + \beta_a & 0 & 0 & 0 \\ a_{41} & a_{42} & 0 & D & 0 & 0 & 0 \\ 0 & 0 & 0 & \eta & -\mu & E & 0 \\ 0 & 0 & 0 & 0 & 0 & 0 & -\mu \end{bmatrix}$$

with:

$$a_{41} = \frac{(1-w)\beta_a \alpha \beta_c}{\kappa + B},$$
$$a_{42} = \frac{(1-w)\beta_a \alpha B + \beta_c}{\kappa + B}.$$

To determine the eigenvalues, we compute the characteristic equation:

$$|J_{E_e} - \lambda I| = 0.$$

Let the corresponding eigenvalues be given by:

$$\lambda_1 = A = -\frac{(1-w)\alpha_c B + \beta_c + \mu + \Psi_c + g}{\kappa + B},$$
$$\lambda_2 = B = -\frac{B\alpha + \beta_a + \mu + \Psi_a}{\kappa + B},$$
$$\lambda_3 = C = -\frac{-\rho(1-m)(\alpha_c + \alpha_a)B + (\beta_a + \beta_c)}{\kappa + B},$$
$$\lambda_4 = D = -(\beta_a + \beta_c + \mu + \varepsilon_1 + \varepsilon_2 + \delta),$$
$$\lambda_5 = E = -\eta,$$
$$\lambda_6 = F = -\mu,$$
$$\lambda_7 = G = -\mu.$$

Thus, the characteristic equation becomes:

$$(A-\lambda)(B-\lambda)(C-\lambda)(D-\lambda)(E-\lambda)(F-\lambda)(G-\lambda) = 0.$$

Since all eigenvalues have negative real parts, i.e., $\mathrm{Re}(\lambda_i) < 0$ for all $i = 1, \ldots, 7$, the trace of J_{E_e} is negative. Hence, the endemic equilibrium point E_e is locally asymptotically stable. □

3.8. Global Stability of the Disease-Free Equilibrium

To establish the global asymptotic stability of the disease-free equilibrium (DFE) of the model defined in eq. (1), we employ the Lyapunov function approach. This method provides a rigorous analytical framework to demonstrate stability through the construction of a Lyapunov function and analysis of its time derivative.

We define the Lyapunov function candidate as:

$$V(t, S_c, S_a, V, I, Q, R, B) = C_1 I + C_2 Q + C_3 B,$$

where $C_1, C_2, C_3 > 0$ are positive constants to be determined.

Taking the time derivative of V, we obtain:

$$\frac{dV}{dt} = C_1 \frac{dI}{dt} + C_2 \frac{dQ}{dt} + C_3 \frac{dB}{dt}.$$

Substituting the corresponding right-hand sides from the model equations gives:

$$\begin{aligned}\frac{dV}{dt} = C_1 \Big[&(1-w)(\gamma_c B + \beta_c I)S_c + (1-w)(\gamma_a B + \beta_a I)S_a \\ &+ \rho(1-m)\left((\gamma_a + \gamma_c)B + (\beta_a + \beta_c)I\right) \\ &- (\mu + \varepsilon_1 + \varepsilon_2 + \delta)I\Big] \\ &+ C_2\Big[(\varepsilon_1 + \varepsilon_2)I - (\mu + \eta + \delta)Q\Big] \\ &+ C_3\Big[\alpha(1-w)I - \sigma B\Big].\end{aligned}$$

To simplify and bound the expression from above, we estimate the upper bound:

$$\begin{aligned}\frac{dV}{dt} \le\ & C_1\left[(1-w)(\gamma_c B + \beta_c I)S_c + (1-w)(\gamma_a B + \beta_a I)S_a\right] \\ &+ C_1\rho(1-m)(\beta_a + \beta_c)I - C_1(\mu + \varepsilon_1 + \varepsilon_2 + \delta)I \\ &+ C_2(\varepsilon_1 + \varepsilon_2)I - C_2(\mu + \eta + \delta)Q \\ &+ C_3\alpha(1-w)I - C_3\sigma B.\end{aligned}$$

We now assign the following values to constants:

$$S_0 = \frac{\Lambda}{\tau + \omega + \mu}, \quad C_1 = \frac{1}{c + \eta + \mu},$$
$$C_2 = \frac{\beta\Lambda}{(c+\eta+\mu)(\varepsilon + \delta + \mu + r)(\tau + \omega + \mu)}.$$

Substituting into the inequality, we obtain:

$$\frac{dV}{dt} \le \frac{c + \eta + \mu}{c + \eta}\left\{\frac{\beta\Lambda}{(\varepsilon + \delta + \mu + r)(\tau + \omega + \mu)} - 1\right\}.$$

Let us denote the coefficient as Γ, then the inequality becomes:

$$\frac{dV}{dt} \le \Gamma(R_0 - 1),$$

where R_0 is the basic reproduction number.

It is important to note that when $\frac{dV}{dt} = 0$, all trajectories approach the largest invariant set contained in $\{I = Q = B = 0\}$, by LaSalle's Invariance Principle. Therefore, the disease-free equilibrium is globally asymptotically stable whenever $R_0 < 1$.

3.9. Global Stability of the Endemic Equilibrium

Theorem 3. *The Dulac criterion can be used in dynamical systems to demonstrate the non-existence of periodic orbits in a given region of the phase space. This result can be extended to analyze the global stability of an endemic equilibrium.*

Proof. Consider the general dynamical system described by the model in eq. (1). Let the state vector be defined as:

$$X = (S_c, S_a, V, I, Q, R, B),$$

and define the Dulac function as:

$$G = \frac{1}{SE},$$

where S and E are strictly positive differentiable functions on the region of interest.

We compute the divergence of the vector field multiplied by G, i.e., $\nabla \cdot (G\mathbf{F})$, component-wise. Below are the transformed equations:

$$G\frac{dS_c}{dt} = \frac{\Lambda}{SE} - \frac{(\tau + \omega) + \beta I + \mu}{E} + \frac{TB}{SE},$$
$$G\frac{dS_a}{dt} = \frac{\beta I}{E} - \frac{(c + \eta + \mu)}{S},$$
$$G\frac{dV}{dt} = \frac{\tau}{E} + \frac{(c+\eta)}{S} - \frac{(\varepsilon + \delta + r + \mu)I}{SE},$$

$$
\begin{aligned}
G\frac{dI}{dt} &= \frac{\omega}{E} + \frac{(r+\varepsilon)I}{SE} - \frac{\mu R}{SE},\\
G\frac{dQ}{dt} &= \frac{-(T+\mu)B}{SE},\\
G\frac{dR}{dt} &= \frac{\eta Q - \mu R}{SE},\\
G\frac{dB}{dt} &= \frac{\alpha(1-w)I - B\sigma}{SE}.
\end{aligned}
$$

Now, we compute the divergence:

$$
\frac{d(GX)}{dt} = \sum_i \frac{\partial}{\partial x_i}\left(G\frac{dx_i}{dt}\right),
$$

where $x_i \in \{S_c, S_a, V, I, Q, R, B\}$. Summing the partial derivatives gives:

$$
\begin{aligned}
\frac{d(GX)}{dt} &= \frac{\partial}{\partial S}(\cdot) + \frac{\partial}{\partial E}(\cdot) + \cdots + \frac{\partial}{\partial B}(\cdot)\\
&= -\left[\frac{\mu}{SE} + \frac{\omega+\tau+\mu}{SE} + \frac{c+\eta+\mu}{SE} + \frac{\varepsilon+\delta+r+\mu}{SE}\right.\\
&\quad \left. + \frac{\mu}{SE}\right],\\
&= -\left[\frac{2\mu + (\mu+\tau) + (c+\eta+\mu)}{SE}\right] < 0.
\end{aligned}
$$

Since $\frac{d(GX)}{dt} < 0$ throughout the region, by Dulac's Criterion, there exists no closed orbit or periodic solution in the region of interest. □

The absence of closed orbits implies that the endemic equilibrium is globally asymptotically stable. From an epidemiological standpoint, this means the system does not exhibit oscillations in the number of infections, providing a predictable path toward equilibrium, which is favorable for planning control strategies and resource allocation.

3.10. Sensitivity Analysis

The main objective of this section is to evaluate how sensitive the basic reproduction number R_0 is with respect to variations in the model parameters. This is achieved by computing the normalized forward sensitivity index, defined as:

$$
\Upsilon_P^{R_0} = \frac{\partial R_0}{\partial P} \cdot \frac{P}{R_0},
$$

where P denotes any given parameter in the model. This sensitivity index measures the relative change in R_0 resulting from a relative change in parameter P. It is particularly useful in identifying which parameters most significantly impact the transmission dynamics of cholera.

The sensitivity analysis helps prioritize control strategies by highlighting key parameters that strongly influence the spread of the disease. The normalized forward sensitivity indices of R_0 with respect to selected parameters are computed as follows:

$$
\begin{aligned}
\Upsilon_w^{R_0} &= \frac{\partial R_0}{\partial w} \cdot \frac{w}{R_0} = -1.2787,\\
\Upsilon_\delta^{R_0} &= \frac{\partial R_0}{\partial \delta} \cdot \frac{\delta}{R_0} = 0.0280,\\
\Upsilon_\eta^{R_0} &= \frac{\partial R_0}{\partial \eta} \cdot \frac{\eta}{R_0} = 1.0000,\\
\Upsilon_\mu^{R_0} &= \frac{\partial R_0}{\partial \mu} \cdot \frac{\mu}{R_0} = -1.0056 \times 10^{-15},\\
\Upsilon_{\Psi_a}^{R_0} &= \frac{\partial R_0}{\partial \Psi_a} \cdot \frac{\Psi_a}{R_0} = 3.7385 \times 10^{-3},\\
\Upsilon_\rho^{R_0} &= \frac{\partial R_0}{\partial \rho} \cdot \frac{\rho}{R_0} = 2.0000 \times 10^{-4},\\
\Upsilon_{\Psi_c}^{R_0} &= \frac{\partial R_0}{\partial \Psi_c} \cdot \frac{\Psi_c}{R_0} = 2.6101 \times 10^{-3}.
\end{aligned}
$$

From the computed indices, we observe that:

- The parameter η has the most significant **positive** impact on R_0, indicating that increasing η leads to a proportionate increase in R_0.
- The parameter w has a strong **negative** influence on R_0, suggesting that higher values of w contribute to reducing the transmission potential.
- Parameters such as ρ, Ψ_a, and Ψ_c have relatively **small positive** effects on R_0.
- The impact of the natural mortality rate μ is negligible, as indicated by a near-zero sensitivity index.

This analysis highlights that interventions targeting parameters with high sensitivity, such as w and η, can be effective in controlling the spread of cholera.

3.11. Numerical simulation

In this section, we perform numerical simulations of the proposed cholera transmission model by applying the Homotopy Perturbation Method (HPM). This method is employed to construct an iterative scheme that generates approximate solutions to the system of differential equations. The iterative terms for each compartment are determined recursively, allowing us to analyze the behavior and progression of the epidemic over time.

We begin by defining the homotopy perturbation of each compartment equation using the embedding parameter $p \in [0, 1]$. The following correctional functionals are constructed:

$$
\begin{aligned}
&(1-p)\frac{dS_c}{dt} + p\left(\Lambda_c - (1-w)[\gamma_c B + \beta_c I]S_c - (\mu+\varphi_c)S_c\right.\\
&\qquad \left. - gS_c\right),\\
&(1-p)\frac{dS_a}{dt} + p\left(\Lambda_a - (1-w)[\gamma_a B + \beta_a I]S_a - (\mu+\varphi_a)S_a\right.\\
&\qquad \left. - gS_a\right),\\
&(1-p)\frac{dV}{dt} + p\left(\varphi_c S_c + \varphi_a S_a - p(1-m)[(\gamma_c+\gamma_a)B\right.\\
&\qquad \left. + (\beta_c+\beta_a)I]V - \mu V\right),\\
&(1-p)\frac{dI}{dt} + p\left((1-w)[\gamma_c B + \beta_c I]S_c + (1-w)[\gamma_a B + \beta_a I]S_a\right.\\
&\qquad \left. + \rho(1-m)[(\gamma_a+\gamma_c)B + (\beta_a+\beta_c)I] - AI\right),\\
&(1-p)\frac{dQ}{dt} + p\left((\varepsilon_1+\varepsilon_2)I - (\mu+\eta+\delta)Q\right),\\
&(1-p)\frac{dR}{dt} + p\left(\eta Q - \mu R\right),\\
&(1-p)\frac{dB}{dt} + p\left(\alpha(1-w)I - \sigma B\right).
\end{aligned}
$$

Assuming the following perturbation series for each state vari-

able:

$$S_c(t) = \sum_{k=0}^{\infty} p^k s_{c,k}(t), \quad S_a(t) = \sum_{k=0}^{\infty} p^k s_{a,k}(t),$$
$$V(t) = \sum_{k=0}^{\infty} p^k v_k(t), \quad I(t) = \sum_{k=0}^{\infty} p^k i_k(t),$$
$$Q(t) = \sum_{k=0}^{\infty} p^k q_k(t), \quad R(t) = \sum_{k=0}^{\infty} p^k r_k(t),$$
$$B(t) = \sum_{k=0}^{\infty} p^k b_k(t).$$

At zeroth order ($n = 0$), we obtain:

$$\frac{ds_{c,0}}{dt} = 0, \quad \frac{ds_{a,0}}{dt} = 0, \quad \frac{dv_0}{dt} = 0, \quad \frac{di_0}{dt} = 0,$$
$$\frac{dq_0}{dt} = 0, \quad \frac{dr_0}{dt} = 0, \quad \frac{db_0}{dt} = 0.$$

Using initial conditions:

$$s_{c,0}(0) = s_{c,0}, \quad s_{a,0}(0) = s_{a,0}, \quad v_0(0) = v_0, \quad i_0(0) = i_0,$$
$$q_0(0) = q_0, \quad r_0(0) = r_0, \quad b_0(0) = b_0,$$

the first-order and higher-order approximations can be calculated accordingly.

Then, the first iteration yields:

$$S_{1c}(t) = (\Lambda_c + \beta - (\tau + \omega)s_0 r_0 + T - \mu)t + s_0,$$
$$S_{1a}(t) = (\Lambda_a + \beta - (\tau + \omega)s_0 r_0 + T - \mu)t + s_0,$$
$$V_1(t) = (\beta s_0 - (c + \eta + \mu)e_0)t + e_0,$$
$$I_1(t) = (\tau s_0 e_0 + (c + \eta)r_0 i_0 - (\varepsilon + \delta + r + \mu))t + i_0,$$
$$Q_1(t) = (\omega s_0 + (r + \varepsilon)e_0 i_0 - \mu)t + r_0,$$
$$R_1(t) = (\omega s_0 + (r + \varepsilon)e_0 i_0 - \mu)t + r_0,$$
$$B_1(t) = (\omega s_0 + (r + \varepsilon)e_0 i_0 - \mu)t + r_0.$$

At $p = 2$, further iterations give approximate forms such as:

$$S_2(t) = \frac{1}{2}\left(\omega^2 i_0 s_0 + \beta\mu s_0 + 2\tau c r_0 - \varepsilon\mu^2 + \beta\omega T + 2\omega c r \varepsilon^2 + \ldots\right)$$

and so on for $V_2(t)$, $I_2(t)$, $Q_2(t)$, $R_2(t)$, and $B_2(t)$.

Initial Conditions Used:$N = 3179.5$, $S_c(0) = 1245.3$, $S_a(0) = 1001.5$, $V(0) = 202.7$, $I(0) = 0.2537 \times 10^{-1}, Q(0) = 1.271$, $R(0) = 1.6717$, $B(0) = 1.3390, \beta_c = 0.805$, $\beta_a = 0.917$, $\gamma_a = \gamma_c = 2.013 \times 10^{-4}, \delta = 1.6728 \times 10^{-5}$, $w = 0.5$, $\rho = 0.3$, $\mu = 0.0106, r = 0.5314$, $\varepsilon_1 = \frac{1}{15}$, $\varepsilon_2 = 0.7273$, $\tau = 0.0013$, $m = 1.2201$. Resulting Time-Dependent Series Solutions:

$$S_c(t) = 33984.79161 \cdot t^3\rho + 1.203551850 \times 10^7 \cdot t^2\rho + 3.949753669 \times 10^7 \cdot t + 32556143,$$
$$S_a(t) = 33984.79161 \cdot t^3\eta + 1.203551850 \times 10^7 \cdot t^2\eta + 3.949753669 \times 10^7 \cdot t\eta + 32556143,$$
$$V(t) = 1.510660599 \times 10^7 \cdot t^2\eta + 1.382923598 \times 10^7 \cdot t^2\eta + 3.913325188 \times 10^7 \cdot t\eta + 3.255643 \times 10^5,$$
$$I(t) = 22010.97832 \cdot t^2\eta + 11619.78832 \cdot t\eta + 3545,$$
$$Q(t) = 32.95058455 \cdot t^2\eta + 19.72880606 \cdot t\eta + 429,$$
$$R(t) = 82.7372 \cdot t^2\eta + 5.78323 \cdot t\eta + 429,$$
$$B(t) = 8.8932 \cdot t^2\eta + 0.278723 \cdot t\eta + 132.$$

The graphical illustrations of these numerical simulations are presented in Figure 2-Figure 13 to show the dynamic behavior over time.

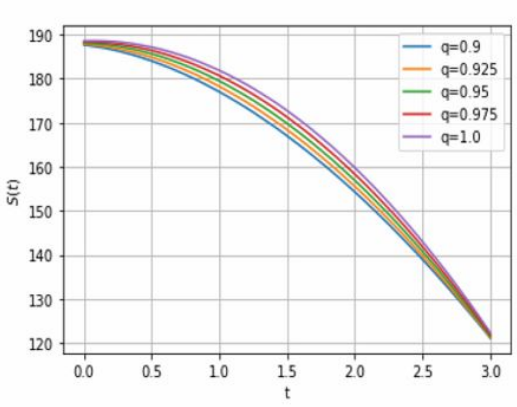

Figure 2. Analysis of vaccination on susceptible population of children

In Figure 2, the susceptible adult population is graphically represented over a span of time, with the vaccination rate of children (plotted on the horizontal axis. As the vaccination rate of children increases, there is a conspicuous downward trend in the susceptible adult population. This trend indicates a clear and direct correlation between child vaccination and the decrease in adult susceptibility to cholera. The visual representation of this correlation underscores the pivotal role that pediatric immunization plays in mitigating the transmission of cholera within communities.

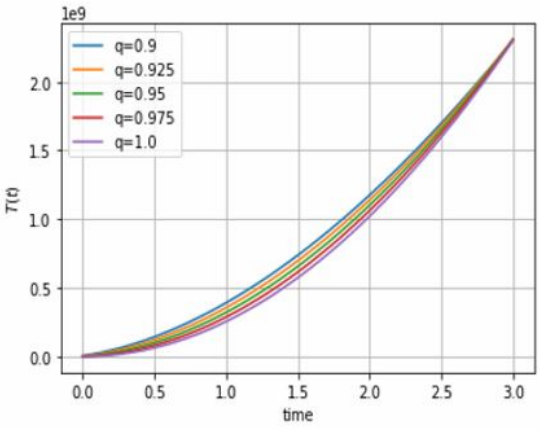

Figure 3. Analysis of vaccination on susceptible population of adult

Figure 3 complements the findings of Figure 2 by depicting the susceptible children population over time, with the vaccination rate of children displayed on the horizontal axis. As the vaccination rate of children increases, Figure 3 illustrates a notable decline in the susceptible children population. This downward

trend in vulnerability among children mirrors the broader strategy of immunization, highlighting the cascading impact of protecting the younger demographic on overall community health.

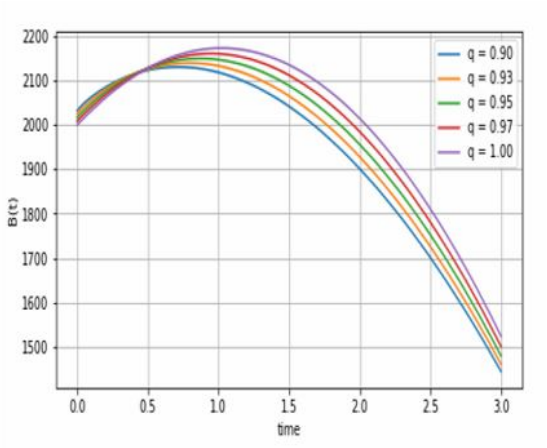

Figure 4. Analysis of vaccination on vaccinated population

Figure 4 likely depicts a trend where as more children receive Cholera vaccinations, the overall proportion of the population that is immunized increases. This trend is essential for achieving herd immunity, a state where a sufficient portion of the population is immune to a disease, effectively preventing its spread. Herd immunity is particularly crucial for diseases like Cholera, which thrive in communities with inadequate sanitation and hygiene practices.

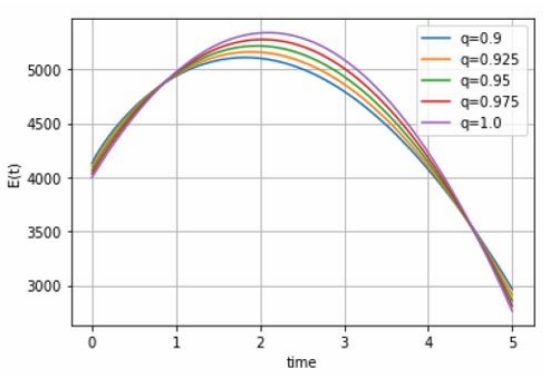

Figure 5. Analysis of vaccination on the infected population

Figure 5 provides further elucidation on the relationship between vaccination and Cholera infection rates by emphasizing the decline in the infected population as the vaccinated population increases within the range of $0 < 1$. This observation underscores the pivotal role of vaccination in mitigating the prevalence of Cholera infections. As more individuals within the population receive vaccinations against Cholera, there is a noticeable decrease in the number of people contracting the disease. This trend is particularly significant in regions where Cholera is endemic or prone to outbreaks.

Figure 6 provides a compelling visualization of the impact of adult vaccination on the prevalence of Cholera infections within a population. It illustrates a notable decrease in the infected population as the vaccination rate of adults rises. This

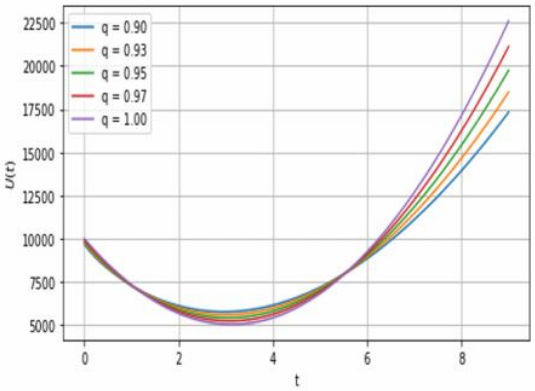

Figure 6. Analysis of vaccination on the children population

observation is crucial as it underscores the significant role that adult vaccination plays in mitigating Cholera transmission and reducing the burden of the disease on public health.

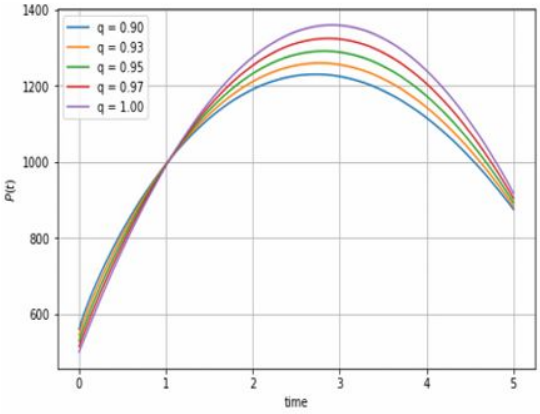

Figure 7. Analysis of vaccination on the Isolated population

Figure 7 presents a comprehensive view of the impact of adult vaccination on the prevalence of Cholera infections, particularly focusing on the dynamics of the isolated population. It illustrates a notable decline in the isolated population as the adult vaccination rate rises. This observation reinforces the idea that adult vaccination not only reduces infection rates but also limits the need for isolating affected individuals, thereby offering significant public health benefits. The isolated population represents individuals who have been diagnosed with Cholera and are subsequently isolated to prevent further transmission of the disease. Isolation measures are essential for containing Cholera outbreaks and preventing its spread within communities. However, these measures can be resource-intensive, socially disruptive, and emotionally taxing for affected individuals and their families.

Figure 8 highlights the significant impact that adult vaccination can have on achieving broad immunity against Cholera. While childhood immunization programs are essential for establishing a foundation of immunity, targeting adults for vaccination can help expedite the process of reaching high vaccination coverage rates within a population. One key advantage of prioritizing adult vaccination is the potential for indirect protection of vulnerable populations, including children. Adults often play a central role in the transmission of infectious diseases within communi-

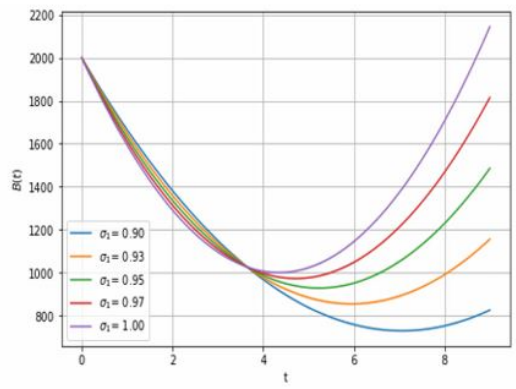

Figure 8. Analysis of vaccination on the susceptible adults

ties. By vaccinating adults against Cholera, public health authorities can reduce the overall prevalence of the disease, thereby creating a protective barrier that extends to individuals who may not have access to or eligibility for vaccination themselves, such as infants or immune compromised individuals.

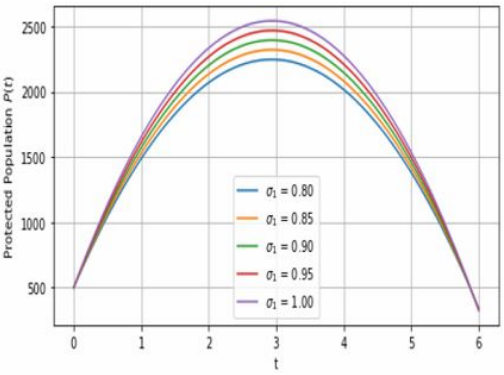

Figure 9. Analysis of waning immunity on the children population

Figure 9 demonstrates that an increase in waning immunity rate corresponds to a rise in the infected population. This highlights the importance of monitoring and addressing waning immunity to prevent a resurgence of Cholera cases.

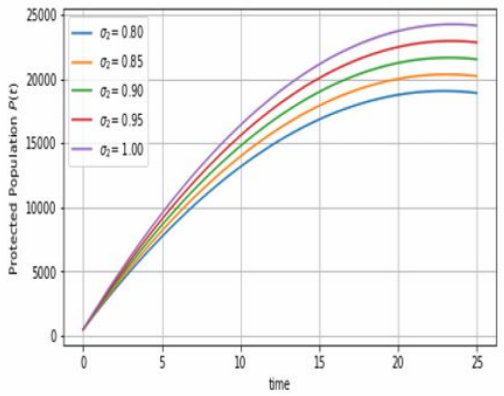

Figure 10. Analysis of waning immunity on the vaccinated population

In Figure 10, the inverse relationship is evident, as the vaccinated population decreases with higher waning immunity rates. This emphasizes the potential need for vaccine boosters to counteract rapid immunity waning and maintain a robust defense against Cholera. Lastly, This brings attention to the crucial role of hygiene in Cholera dynamics.

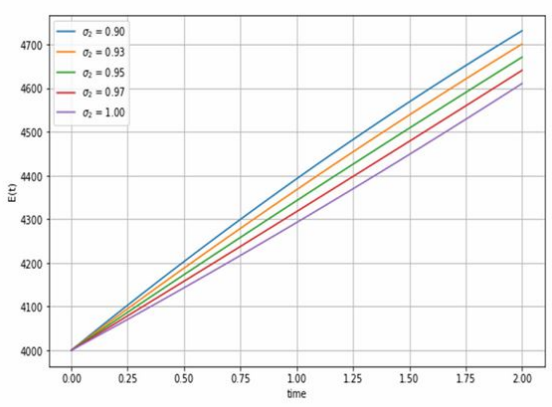

Figure 11. Analysis of hygiene on the susceptible adult population

Figure 11 highlights the rapid escalation in susceptibility to infections with higher hygienic rates, particularly reaching a critical vulnerability level when hygiene practices are at their maximum. This figure likely depicts a graphical representation of data showcasing the relationship between hygiene levels and susceptibility to infectious diseases or conditions. The data would likely indicate that as hygiene practices improve, susceptibility initially decreases, but beyond a certain point, susceptibility begins to increase again, potentially reaching a peak at maximum hygiene levels.

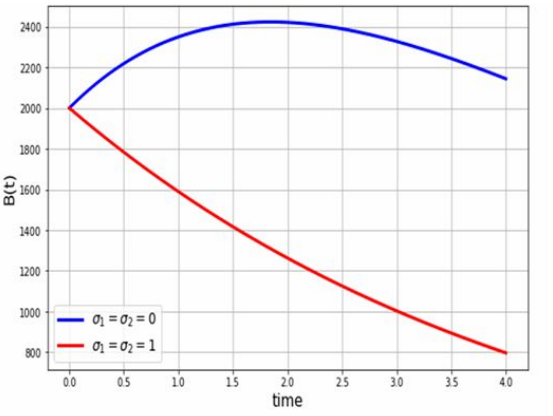

Figure 12. Analysis of hygiene on the susceptible children population

Figure 12 mirrors the trend observed in susceptible children, underlining the critical importance of upholding stringent hygiene practices to safeguard vulnerable populations. This figure likely presents data illustrating the prevalence or incidence rates of infectious diseases or conditions among children who are susceptible due to factors such as age, compromised immune systems, or other underlying health conditions. The data likely

show an increase or fluctuation in the occurrence of these illnesses over time .The emphasis on maintaining hygiene practices underscores the fundamental role of cleanliness and sanitation in preventing the spread of infectious agents. Proper hygiene practices, such as regular hand washing with soap and water, maintaining clean environments, practicing respiratory etiquette (such as covering coughs and sneezes), and avoiding close contact with sick individuals, are essential strategies for reducing the transmission of pathogens.

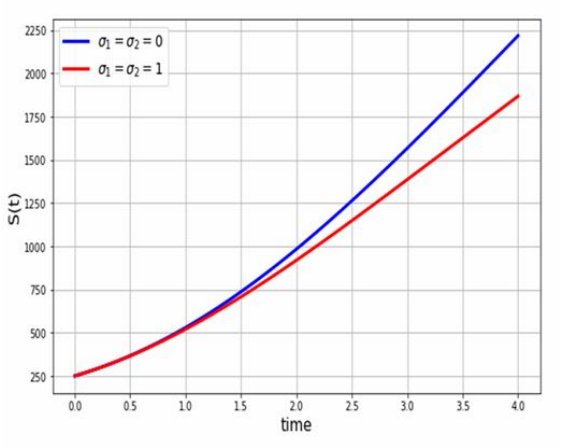

Figure 13. Analysis of hygiene on the bacteria population

Figure 13 provides a compelling illustration of the profound impact of hygiene on reducing bacterial populations. The data likely depict a clear inverse relationship between hygienic practices and the abundance of bacteria, showing a drastic decrease in bacterial populations as hygienic practices increases. This relationship underscores the pivotal role of proper sanitation in creating and maintaining disease-free environments, particularly in the context of preventing the spread of bacterial infections such as cholera. The significant reduction in bacterial populations observed with improved hygiene practices emphasizes the effectiveness of sanitation measures in controlling the proliferation and transmission of pathogens. Hygienic practices such as regular hand washing, proper food handling, safe water storage and treatment, and sanitation infrastructure play crucial roles in limiting the reservoirs and vectors through which bacteria spread, thereby curbing the incidence and severity of infectious diseases.

4. Conclusion

The findings of this study underscore the pivotal role of mathematical modeling in guiding public health policy and designing effective interventions for cholera control. By incorporating vaccine efficacy and age-specific population structure into the modeling framework, this research offers critical insights into the transmission dynamics of cholera and the potential impact of targeted control strategies. The analytical results demonstrate that vaccination campaigns, especially those directed toward particular age groups or implemented with high coverage rates, are highly effective in reducing the incidence of cholera. This emphasizes the value of strategic immunization planning as a cornerstone of disease prevention and mitigation. Furthermore, the study highlights the necessity of continuous surveillance and real-time monitoring systems to facilitate early detection of cholera outbreaks. Early identification of potential epidemic patterns enables swift public health responses, thereby minimizing transmission and preventing large-scale spread. In summary, integrating mathematical modeling with vaccination strategies and robust epidemiological surveillance presents a comprehensive approach to cholera control. These tools collectively enhance decision-making processes and contribute to the development of evidence-based, cost-effective public health interventions.

Author Contributions. **Mutairu K. Kolawole:** Conceptualization, methodology, formal analysis, writing—original draft preparation. **Segun R. Adebayo:** Software, validation, data curation, writing—review and editing. All authors discussed the results and contributed to the final manuscript.

Acknowledgement. The authors are thankful to the editors and reviewers who have supported us in improving this manuscript. We also acknowledge all contributors who assisted in the research and preparation of this work.

Funding. This research received no external funding.

Conflict of interest. The authors declare that there are no conflicts of interest related to this article.

Data availability. Not applicable.

References

[1] M. Kolawole, A. Oluwarotimi, K. Odeyemi, and A. Popoola, "Analysis of Corona-Virus Mathematical Model in Asymptomatic and Symptomatic Cases with Vaccine using Homotopy Perturbation Method," *Journal of Applied Computer Science and Mathematics*, vol. 17, no. 1, pp. 20–27, 2023.

[2] M. Akhtar et al., "Kinetics of antibody-secreting cell and fecal IgA responses after oral cholera vaccination in different age groups in a cholera endemic country," *Vaccine*, vol. 35, no. 2, pp. 321–328, 2017.

[3] B. O. Akin-awoniran, M. K. Kolawole, and K. A. Odeyemi, "On the Numerical Analysis of the Effect of Vaccine on Measles using Variational Iteration Method," *Jurnal Diferensial*, vol. 5, no. 2, 2023. doi: 10.35508/jd.v5i2.

[4] I. Baba, U. Humphries, and F. Rihan, "Role of Vaccines in Controlling the Spread of COVID-19: A Fractional-Order Model," *Vaccines*, vol. 11, no. 1, p. 145, 2023.

[5] C. C. Chisenga et al., "Assessment of the influence of ABO blood groups on oral cholera vaccine immunogenicity in a cholera endemic area in Zambia," *BMC Public Health*, 2023.

[6] S. Ganjefar and S. Rezaei, "Modified homotopy perturbation method for optimal control problems using the Padé approximant," *Applied Mathematical Modelling*, vol. 40, no. 15–16, pp. 7062–7081, 2016.

[7] Ader *et al.*, "Homotopy Perturbation Method for Boundary Value Problems with Delay Differential Equations," *ASM Science Journal*, 2024.

[8] T. Hui Xian, S. Parasuraman, M. Ravichandran, and G. Prabhakaran, "Dual-Use Vaccine for Diarrhoeal Diseases: Cross-Protective Immunogenicity of a Cold-Chain-Free, Live-Attenuated, Oral Cholera Vaccine against Enterotoxigenic Escherichia coli (ETEC) Challenge in BALB/c Mice," *Vaccines*, vol. 10, no. 12, p. 2161, 2022.

[9] S. Iqbal, F. Martínez, M. K. A. Kaabar, and M. E. Samei, "A novel Elzaki transform homotopy perturbation method for solving time-fractional nonlinear partial differential equations," *Boundary Value Problems*, vol. 2022, no. 1, 2022. doi: 10.1186/s13661-022-01673-3.

[10] J.-H. Kim, V. Mogasale, C. Burgess, and T. F. Wierzba, "Impact of oral cholera vaccines in cholera-endemic countries: A mathematical modeling study," *Vaccine*, vol. 34, no. 18, pp. 2113–2120, 2016.

[11] J. Liang, L. Liu, and Z. Jin, "A reaction-diffusion-advection logistic model with a free boundary in heterogeneous environment," *Boundary Value Problems*, vol. 2016, no. 1, 2016.

[12] E. I. Mahmoud and T. S. Aleroev, "Boundary Value Problem of Space-Time Fractional Advection Diffusion Equation," *Mathematics*, vol. 10, no. 17, p. 3160, 2022.

[13] S. S. Musa, S. Zhao, M. H. Wang, A. G. Habib, and U. T. Mustapha, "Estimation of exponential growth rate and basic reproduction number of the coronavirus disease 2019 (COVID-19) in Africa," *World Health Organization, Coronavirus Disease*, 2020.

[14] M. Kolawole, K. Odeyemi, K. Bashiru, and A. Popoola, "An Approximate Solution of Fractional Order Epidemic Model of Typhoid using Homotopy Perturbation Method," *UNIOSUN Journal of Engineering and Environmental Sciences*, vol. 5, no. 1, 2023. doi: 10.36108/ujees/3202.50.0180.

[15] N. Abdul, L. Yahya, R. Resmawan, and A. Nuha, "Dynamic analysis of the mathematical model of the spread of cholera with vaccination strategies," *BAREKENG: J. Math. & App.*, vol. 16, no. 1, 2022. doi: 10.30598/barekengvol16iss1pp279-290.

[16] M. K. Kolawole, M. O. Olayiwola, and K. A. Odeyemi, "Extensive Analysis and Projection of the Impact of High-Risk Immunity Using a Mathematical Model That Incorporates a Convex Incidence Rate of Multiple Covid-19 Exposures," *Cankaya University Journal of Science and Engineering*, vol. 20, no. 2, pp. 107–128, 2023.

[17] M. K. Kolawole, M. O. Olayiwola, and K. A. Odeyemi, "Extensive Analysis and Projection of the Impact of High-Risk Immunity Using a Mathematical Model That Incorporates a Convex Incidence Rate of Multiple Covid-19 Exposures," *Cankaya University Journal of Science and Engineering*, vol. 20, no. 2, pp. 107–128, 2023.

[18] M. K. Kolawole, M. O. Olayiwola, and K. A. Odeyemi, "Conceptual analysis of the combined effects of vaccination, therapeutic actions, and human subjection to physical constraint in reducing the prevalence of COVID-19 using the homotopy perturbation method," *Beni-Suef University Journal of Basic and Applied Sciences*, vol. 12, no. 10, 2023. doi: 10.1186/s43088-023-00343-2.

[19] M. K. Kolawole, K. A. Odeyemi, K. A. Bashiru, and A. O. Oladapo, "Dynamical Analysis and Control Strategies for Capturing the Spread of Covid-19," *Tanzania Journal of Science*, vol. 48, no. 3, pp. 680–690, 2022.

[20] M. Kolawole, A. Oluwarotimi, K. Odeyemi, and A. Popoola, "Analysis of Corona-Virus Mathematical Model in Asymptomatic and Symptomatic Cases with Vaccine using Homotopy Perturbation Method," *Journal of Applied Computer Science and Mathematics*, vol. 17, no. 1, pp. 20–27, 2023.

[21] P. Riyapan, S. E. Shuaib, and A. Intarasit, "A Mathematical Model of COVID-19 Pandemic: A Case Study of Bangkok, Thailand," *Journal of Mathematics*, vol. 2021, Art. ID 6664483, 2021. doi: 10.1155/2021/6664483.

[22] S. Saha, G. P. Samanta, and J. J. Nieto, "Epidemic model of COVID-19 outbreak by Center for Systems Science and Engineering at Johns Hopkins University," *COVID19*, 2020.

[23] P. A. Zegeling, "A homotopy perturbation method for fractional-order advection-diffusion-reaction boundary-value problems," *Applied Mathematical Modelling*, vol. 47, pp. 425–441, 2017.